



Design Method of Differential Cascading for Dual-Stator Brushless Doubly-Fed Induction Wind Generator With Staggered Dual Cage Rotor

Yu Zeng, Ming Cheng*, Xiaoming Yan and Changguo Zhang

School of Electrical Engineering, Southeast University, Nanjing, China

OPEN ACCESS

Edited by:

Liansong Xiong,
Nanjing Institute of Technology (NJIT),
China

Reviewed by:

Qingsong Wang,
Southeast University, China
Ramtin Sadeghi,
IAU, Iran
Lei Liu,
Xi'an Jiaotong University, China

*Correspondence:

Ming Cheng
mcheng@seu.edu.cn

Specialty section:

This article was submitted to
Process and Energy Systems
Engineering,
a section of the journal
Frontiers in Energy Research

Received: 29 July 2021

Accepted: 31 August 2021

Published: 15 September 2021

Citation:

Zeng Y, Cheng M, Yan X and Zhang C
(2021) Design Method of Differential
Cascading for Dual-Stator Brushless
Doubly-Fed Induction Wind Generator
With Staggered Dual Cage Rotor.
Front. Energy Res. 9:749424.
doi: 10.3389/fenrg.2021.749424

This article proposes a new differential-cascading-based dual-stator brushless doubly-fed induction machine with a staggered dual cage rotor. Conventional differential mode of the brushless doubly-fed machine with cage rotor suffers from the low number of rotor bars because of the low equivalent synchronous pole pairs of $|p_1 - p_2|$, and thus, severe rotor flux leakage, low capacity of magnetic field conversion of the rotor and low efficiency. To overcome the obstacle of the excessive harmonics of the rotor, a design method based on the differential cascading is proposed which enables the cage rotor with a high number of conductor bars even in the case of low pole pairs of $|p_1 - p_2|$, hence the greatly reduced rotor leakage inductance and enhanced performance of the machine. The rotating magneto-motive force theory is applied to derive the interconnection rule of the staggered dual cage rotor, and meanwhile, the corresponding examples are illustrated. The performance comparisons between the differential cascading and the sum cascading based on the proposed machine are carried out. The results show that the proposed machine based on the differential cascading obtains higher power densities comparing to the sum cascading at the region of sub-natural synchronous speed, while its drawback is the increment of the loss due to the high rotor frequency, gaining lower efficiencies at the region of super-natural synchronous speed.

Keywords: brushless doubly-fed generator, wind turbine, generators, conductors, cage rotors

INTRODUCTION

Brushless doubly-fed machines (BDFMs), as the alternative to the conventional doubly-fed induction machine (DFIM) (Yin, 2021; Zhang et al., 2021), offer increased reliability and low maintenance due to the elimination of the brushes and slip-rings (Okedu et al., 2021), showing the promising prospects in the fields of variable speed constant frequency system (VSCF) such as the on-shore and off-shore wind power generation system (Cheng and Zhu, 2014; Han et al., 2018; Xiong et al., 2020). The critical technology of the BDFM is the structure design of the rotor which determines the capacity of the magnetic field conversion between the power subsystem and the control subsystem. Therefore, lots of feasible rotor topologies have been investigated by researchers from academia and industry like the nested-loop rotor (Shao et al., 2012), the wound rotor (Ruviano et al., 2011), and the reluctance rotor (Zhang et al., 2019). A relatively new machine with dual-stators and dual-rotors called the dual-stator brushless doubly-fed induction machine (DS-BDFIM) has been developed in recent years which offers the merits of low harmful harmonics and good winding insulation.

However, the capacity of the magnetic field conversion for the cascaded wound rotor seems to be low due to the relatively high rotor resistance (Zeng et al., 2021). To reduce the copper loss of the rotor and improve the efficiency of the DS-BDFIM, back to the structure of the cage rotor is a potential solution. Consequently, in this article, the DS-BDFIM with cage rotor is studied.

No matter what kinds of rotor structures used in previous literature, two main magnetic fields produced by the rotor are generally opposite, constructing the synchronous machine with equivalently (p_1+p_2) pole pairs and the natural synchronous speed of the BDFM is $60f_1/(p_1 + p_2)$. The operation principle is the so-called sum mode. By that analogy, if a magnetic field of the rotor rotates in the same direction with respect to the other one, the natural synchronous speed of the BDFM is determined by $60f_1/|p_1-p_2|$ and the pole pairs are equivalent to be $|p_1-p_2|$ which has been pointed out in (Williamson et al., 1997), namely, the differential mode of the BDFM. Since $n \propto 1/p$ (where p indicates the $(p_1 + p_2)$ in the sum mode of the BDFM and the $|p_1-p_2|$ in the differential mode of the BDFM, while n is the synchronous speed of the machine), the synchronous speed of the differential mode of the BDFM is higher than the sum mode one. The higher synchronous speed owns the increased power density of the machine. It means that the differential mode of the BDFM has the potential ability of higher power density comparing to the sum mode of the BDFM. Moreover, a wider range of speed for the differential-mode-based BDFM is significantly beneficial for the wind power generation in a complex environment.

The key to restricting the development of the differential mode of the BDFM is the severe rotor flux leakage. In the early study (Williamson et al., 1997), the cage rotor is utilized for the differential-mode-based BDFM, but the number of rotor bars is too low owing to the low pole pairs of $|p_1-p_2|$, resulting in excessive harmonics and the large rotor leakage inductance. Although Robert P. C. reported in (Roberts, 2004) that the rotor leakage inductance can be declined when the appropriate design method is adopted, there is little hope of success for the nested-loop and the reluctance rotors (Li et al., 2019). To solve the problem of the excessive harmonics of the rotor, Cheng Y. utilized the special design method for the wound rotor to reduce the harmonic content (Cheng et al., 2020). The reasonable wound winding design indeed can reduce the rotor harmonics, however, the high rotor resistance is a prevalent obstacle that the wound rotor usually experiences, leading to high copper loss. Further, the rotor current frequency of the differential-mode-based BDFM is much higher than the sum mode one, leading to the increased rotor copper loss and iron loss (Pan et al., 2020). To overcome the drawbacks of the wound rotor, the cage rotor structure with low resistance should be reconsidered. BDFMs can be divided into two categories in terms of the operating principle, namely, the class of modulation and the class of cascaded (Zeng et al., 2020). Williamson S. verified that the differential mode is not appropriate to the nested-loop rotor with the modulation principle (Williamson et al., 1997). Therefore, the cascaded cage rotor is supposed to be investigated to realize the purpose of the rotor with a large number of conductor bars under low pole

pairs. The problem that should be addressed now is the interconnection of the rotor conductor bars to produce the same direction of rotation for two main magnetic fields and build so-called differential cascading (DC).

In this article, the design method of DC for the DS-BDFIM with a staggered dual cage rotor (DS-BDFIM-SDCR) is proposed. The number of conductor bars of DS-BDFIM-SDCR based on the DC is in accordance with the sum cascading (SC) one which means the number of conductor bars large even with the pole pairs of $|p_1-p_2|$, hence the greatly reduced rotor leakage inductance and improved performance of the machine. The theoretical derivation of the interconnection rule of the DS-BDFIM-SDCR based on the DC is developed in *Design Method of DC*. The specific pole/slot combinations are introduced in *Slot/Pole Combinations of DS-BDFIM-SDCR* in detail. The advantage of the wide speed range and the disadvantage of the increased loss are discussed in *Comparison of DS-BDFIM-SDCR with DC and SC*, and meanwhile, the finite element (FE) models of the DC and SC modes of the DS-BDFIM-SDCR are established to compare their performances. Finally, the vital conclusion is drawn in *Conclusion*.

DESIGN METHOD OF DC

Structure of DS-BDFIM-SDCR

The DS-BDFIM-SDCR consists of the outer stator, the inner stator and the cup-shaped rotor as shown in **Figures 1A,B**. The power winding (PW) is placed in the slotted outer stator to output power, while the control winding (CW) is wrapped around the inner stator to account for the slip power. The cup-shaped rotor is made of the inner cage rotor, the outer cage rotor and the non-magnetic support in between, termed as the SDCR. The non-magnetic support enables the electric coupling instead of the magnetic coupling between the inner and outer cage rotors, achieving the cascaded principle rather than the modulation one. More details about the SDCR is presented in **Figure 1C**, showing that on the one end the conductor bars of the inner and outer cages are shorted-circuited by two end rings, whereas on the other end they are interconnected in a staggered way to form the same rotating magnetic fields, namely, the DC. It is worth mentioning that the real 3-dimension topology of 40 staggered conductor bars (40 slots of the rotor for the proposed machine) is a little bit complex, and hence, the simplified view (only for reference) is provided for a clear illustration. The design parameters of the proposed DS-BDFIM-SDCR are tabulated in **Table 1**. Obviously, the equivalent synchronous 1 pole pair and the 40 slots of the rotor (namely, the number of the conductor bars) heavily reduce the rotor flux leakage and harmonics. Therefore, the obstacle of the differential mode for the conventional BDFIM with the cage rotor is removed in a sense.

Derivation of Interconnection Rule for SDCR

The cage winding can be treated as a balanced multi-phase winding whose phase and slot numbers are the same. The number of conductors for each phase is 1. Since the

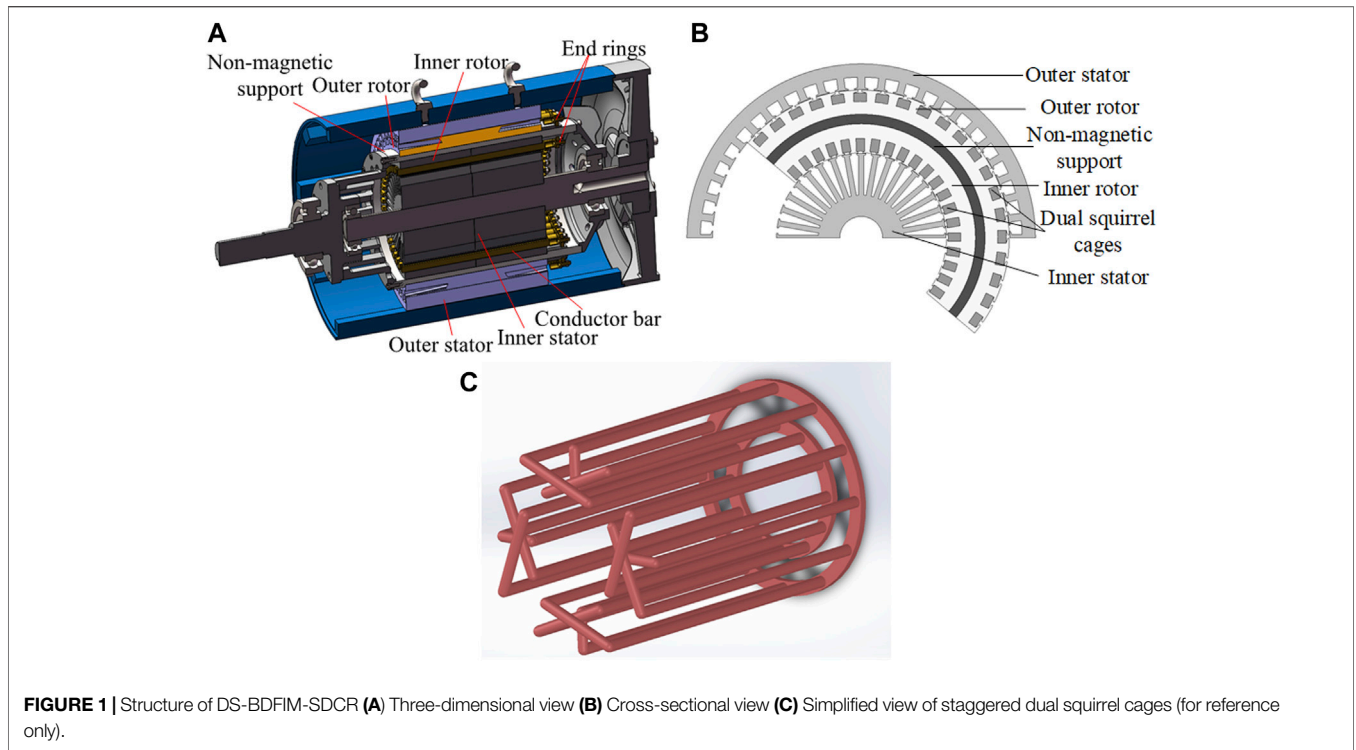


FIGURE 1 | Structure of DS-BDFIM-SDCR (A) Three-dimensional view (B) Cross-sectional view (C) Simplified view of staggered dual squirrel cages (for reference only).

TABLE 1 | Specification of proposed DS-BDFIM-SDCR

Design parameters	Values
PW and CW pole pairs	2, 1
Slot number of outer stator and outer rotor	48, 40
Slot number of inner rotor and inner stator	40, 36
Rated PW voltage (V)	220
Rated frequencies of PW and CW (Hz)	50, 12.5
Rated speed (r/min)	3,750
Outer and inner diameters of outer stator (mm)	325, 277
Outer and inner diameters of outer rotor (mm)	276, 231
Thickness of non-magnetic support (mm)	9
Outer and inner diameters of inner rotor (mm)	213, 159
Outer and inner diameters of inner stator (mm)	158, 40
Axial length of stator core (mm)	246

conductors are symmetrically distributed, the current amplitudes and the current frequencies of the conductor bars are the same. However, their phase angles are different. The electric phase angle of the current for the adjacent conductor bars is defined as

$$\alpha = \frac{2\pi p_c}{Z_c} \quad (1)$$

And because of the conductor bars arranged symmetrically along the circumference of the rotor in space, the adjacent conductor bars differ a phase angle β in space

$$\beta = \frac{2\pi p_p}{Z_p} \quad (2)$$

where p_p and p_c are respectively given as the pole pairs of the PW and the CW, while Z_p and Z_c represent the number of slots

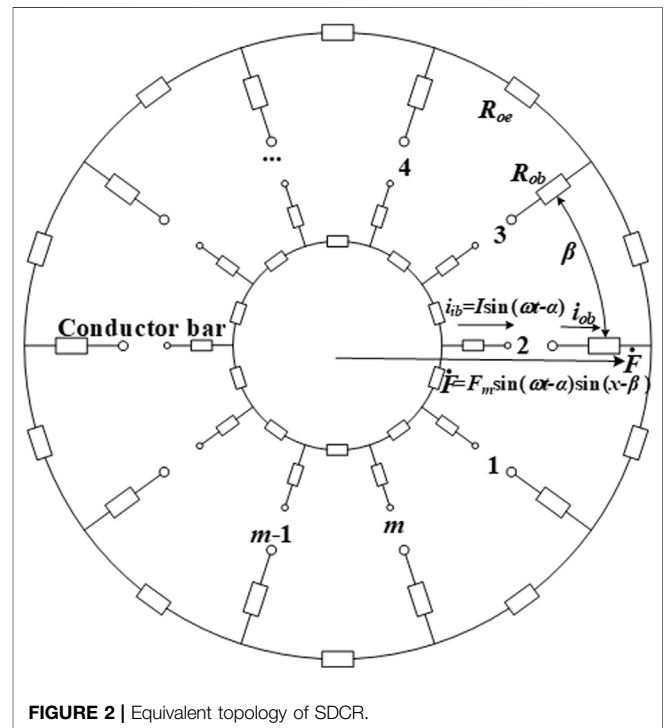


FIGURE 2 | Equivalent topology of SDCR.

of the outer and inner rotors. The equivalent topology of the SDCR is given in Figure 2, explaining the relation of inner and outer cages.

If the balanced m phases currents are injected into the balanced m phases cage winding, the fundamental magnetomotive forces (MMFs) are given by

$$\begin{cases} f_1 = F_m \sin(\omega t) \sin(x) \\ f_2 = F_m \sin(\omega t - \alpha) \sin(x - \beta) \\ f_3 = F_m \sin(\omega t - 2\alpha) \sin(x - 2\beta) \\ \vdots \\ f_m = F_m \sin[\omega t - (m-1)\alpha] \sin[x - (m-1)\beta] \end{cases} \quad (3)$$

where F_m is the amplitude of the fundamental MMF.

Making a summation of all MMFs from Eq. 3 and using the product-to-sum formulas of the trigonometric function, the synthetic MMF can be derived as

$$f = \frac{1}{2} F_m \begin{cases} \cos(\omega t - x) [1 + \cos(\alpha - \beta) + \cos[2(\alpha - \beta)] + \dots + \cos[(m-1)(\alpha - \beta)] \\ + \sin(\omega t - x) [\sin(\alpha - \beta) + \sin[2(\alpha - \beta)] + \dots + \sin[(m-1)(\alpha - \beta)]] \\ - \cos(\omega t + x) [1 + \cos(\alpha + \beta) + \cos[2(\alpha + \beta)] + \dots + \cos[(m-1)(\alpha + \beta)]] \\ - \sin(\omega t + x) [\sin(\alpha + \beta) + \sin[2(\alpha + \beta)] + \dots + \sin[(m-1)(\alpha + \beta)]] \end{cases} \quad (4)$$

On the basis of Euler's formula

$$e^{i\theta} = \cos(\theta) + i \sin(\theta) \quad (5)$$

Eqs. 6, 7 are easily derived

$$\cos(\theta) = \frac{e^{i\theta} + e^{-i\theta}}{2} \quad (6)$$

$$\sin(\theta) = \frac{e^{i\theta} - e^{-i\theta}}{2i} \quad (7)$$

According to Eqs. 4, 6, 7, the synthetic MMF is rewritten as

$$f = \frac{1}{2} F_m \begin{cases} \cos(\omega t - x) \left[\frac{1 + e^{i(\alpha-\beta)} + e^{i2(\alpha-\beta)} + \dots + e^{i(m-1)(\alpha-\beta)}}{2} \right. \\ \left. + \frac{1 + e^{-i(\alpha-\beta)} + e^{-i2(\alpha-\beta)} + \dots + e^{-i(m-1)(\alpha-\beta)}}{2} \right] \\ + \sin(\omega t - x) \left[\frac{e^{i(\alpha-\beta)} + e^{i2(\alpha-\beta)} + \dots + e^{i(m-1)(\alpha-\beta)}}{2i} \right. \\ \left. - \frac{e^{-i(\alpha-\beta)} + e^{-i2(\alpha-\beta)} + \dots + e^{-i(m-1)(\alpha-\beta)}}{2i} \right] \\ - \cos(\omega t + x) \left[\frac{1 + e^{i(\alpha+\beta)} + e^{i2(\alpha+\beta)} + \dots + e^{i(m-1)(\alpha+\beta)}}{2} \right. \\ \left. + \frac{1 + e^{-i(\alpha+\beta)} + e^{-i2(\alpha+\beta)} + \dots + e^{-i(m-1)(\alpha+\beta)}}{2} \right] \\ - \sin(\omega t + x) \left[\frac{e^{i(\alpha+\beta)} + e^{i2(\alpha+\beta)} + \dots + e^{i(m-1)(\alpha+\beta)}}{2i} \right. \\ \left. - \frac{e^{-i(\alpha+\beta)} + e^{-i2(\alpha+\beta)} + \dots + e^{-i(m-1)(\alpha+\beta)}}{2i} \right] \end{cases} \quad (8)$$

Four common ratios are given as

$$\begin{cases} q_1 = e^{i(\alpha-\beta)} = 1 \\ q_2 = e^{-i(\alpha-\beta)} = 1 \\ q_3 = e^{i(\alpha+\beta)} \neq 1 \\ q_4 = e^{-i(\alpha+\beta)} \neq 1 \end{cases} \quad (9)$$

Substituting Eq. 9 into Eq. 8, the synthetic MMF is finally given by

$$f = \frac{1}{2} F_m \begin{cases} \cos(\omega t - x) \left(\frac{1 + 1 + \dots + 1}{2} + \frac{1 + 1 + \dots + 1}{2} \right) \\ + \sin(\omega t - x) \left(\frac{1 + 1 + \dots + 1}{2i} - \frac{1 + 1 + \dots + 1}{2i} \right) \\ - \cos(\omega t + x) \left(\frac{1}{2} \frac{1 - 1}{1 - e^{i(\alpha+\beta)}} + \frac{1}{2} \frac{1 - 1}{1 - e^{-i(\alpha+\beta)}} \right) \\ - \sin(\omega t + x) \left(\frac{1}{2i} \frac{e^{i(\alpha+\beta)} - 1}{1 - e^{i(\alpha+\beta)}} - \frac{1}{2i} \frac{e^{-i(\alpha+\beta)} - 1}{1 - e^{-i(\alpha+\beta)}} \right) \end{cases} \quad (10)$$

Eq. 10 can be simplified further

$$f = \frac{1}{2} F_m \begin{cases} \cos(\omega t - x) \left(\frac{m}{2} + \frac{m}{2} \right) + \sin(\omega t - x) \left(\frac{m-1}{2i} - \frac{m-1}{2i} \right) \\ - \cos(\omega t + x) (0 + 0) - \sin(\omega t + x) \left(-\frac{1}{2i} + \frac{1}{2i} \right) \end{cases} = \frac{m}{2} F_m \cos(\omega t - x) \quad (11)$$

where $\omega t - x$ is defined as the positive rotation of the magnetic field, while $\omega t + x$ represents the negative rotation. The physical meaning of Eq. 11 is that the inner and outer conductor bars are interconnected in a positive-phase sequence to produce the same rotation direction of the magnetic fields of the rotor currents, namely, the so-called DC.

SLOT/POLE COMBINATIONS OF DS-BDFIM-SDCR

α and β represent the electric phase angles of the slots in the CW and the PW sides and they are should be the same under the DC

$$\beta = \alpha = \frac{2\pi p_p}{Z_p} = \frac{2\pi p_c}{Z_c} \quad (12)$$

Then, the requirement of the slot/pole combination of the PW and CW is gained

$$p_p Z_c = p_c Z_p \quad (13)$$

The steady-state speed of the DS-BDFIM-SDCR based on the DC is given by

$$n_r = \frac{60(f_p \pm f_c)}{|p_p - p_c|} \quad (14)$$

From Eq. 14, the pole pairs of the PW and the CW cannot be the same

$$p_p \neq p_c \quad (15)$$

Then, from Eqs. 13, 15, only one case should be considered

$$p_p = k p_c \quad Z_p = k Z_c \quad (16)$$

where k belongs to the positive integer (2, 3, 4...) and the improper fraction (3/2, 5/4, 6/5...) if p_p is larger than p_c , while the k is the proper fraction (1/2, 1/3, 2/3...) when the p_p is lower than p_c .

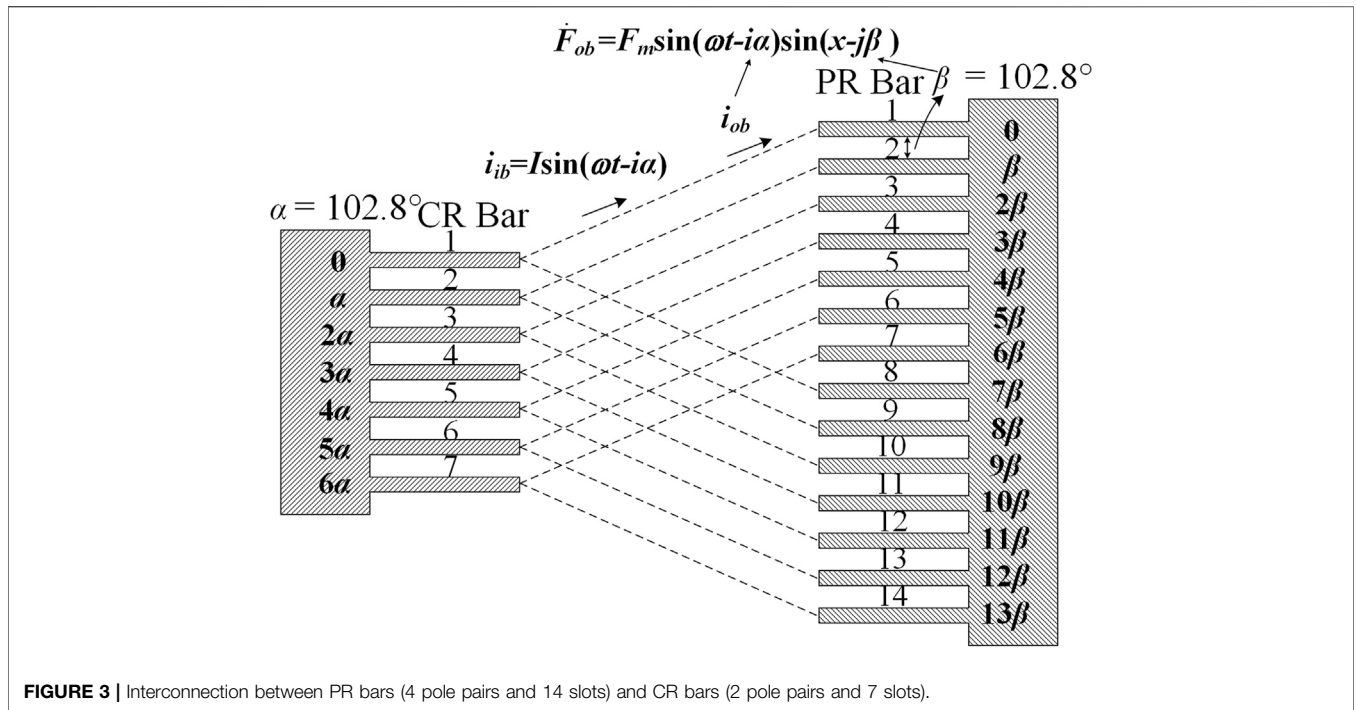


FIGURE 3 | Interconnection between PR bars (4 pole pairs and 14 slots) and CR bars (2 pole pairs and 7 slots).

Additionally, one more case also should be discussed

$$p_p = kp_c \quad Z_p = Z_c \quad (17)$$

It can be known that Eq. 17 mismatches the condition of Eq. 13, but a technique called the virtual slot method (VSM) is proposed in this article to convert the SDCR into a joinable way. Hereto, most possible slot/pole combinations have been covered by Eqs. 16, 17, and then the examples are introduced to establish the DS-BDFIM-SDCR based on the DC.

$p_p = kp_c$ and $Z_p = kZ_c$

When the pole pairs and the rotor slots of the power rotor (PR) are the k multiples of the control rotor (CR), the conductor bars of the PR and CR are cannot directly be connected due to their different slots. The solution is that k conductor bars in a slot in parallel connect to the k slots on the other side where one slot places one conductor bar. Generally, the rotor with the lower number of slots has k conductor bars in one slot, while the rotor with the higher number of slots only arranges one conductor bar in one slot.

An example of the PR with 4 pole pairs (14 slots) and the CR with 2 pole pairs (7 slots) is given in Figure 3, showing the interconnection between PR and CR bars. Since the electrical phase angles α and β are calculated to be 102.8° , the PR and CR are interconnected under the guidance of Eq. 12. Two conductor bars should be settled in one slot of the CR, connecting two slots of the PR. Table 2 tabulates the details of the interconnection between the PR and the CR. The conductor bars of the PR and the CR should be divided into two groups ($k = 2$), namely groups I and II, to normalize the interconnection. Each group consists of 7 conductor bars which occupy a 4π electric period owing to the electrical phase angles α and β of 102.8° . On the basis of Eq. 12, the PR and CR bars

TABLE 2 | Interconnection between PR and CR bars under PR with 4 pole pairs and 14 slots, CR with 2 pole pairs and 7 slots.

	CR		PR	
Pole pair	2		4	
Slot	7		14	
Electric phase angle	102.8°		102.8°	
Group I	Bar No	α	Bar No	β
	1	0	1	0
	2	102.8	2	102.8
	3	205.6	3	205.6
	4	308.4	4	308.4
	5	411.2	5	411.2
	6	514	6	514
	7	616.8	7	616.8
Group II	1	0	8	719.6
	2	102.8	9	822.4
	3	205.6	10	925.2
	4	308.4	11	1,028
	5	411.2	12	1,130.8
	6	514	13	1,233.6
	7	616.8	14	1,336.4

of the same group are interconnected correspondingly in a positive-phase sequence way to building the DC.

Figure 4 displays that the pole pairs of the PR and the CR are given by 3 and 2, while the slots of the PR and the CR are 12 and 8, respectively. The PR and CR bars are interconnected according to Eq. 12 under k of improper fraction $3/2$. Since the number of slots of the PR is not an integral multiple of the CR ones, the areas of the conductor bars for the PR and CR cannot be the same. Therefore, a slot of the CR should be placed in two paralleled conductor bars, one of which has 1 per-unit-area and the other is

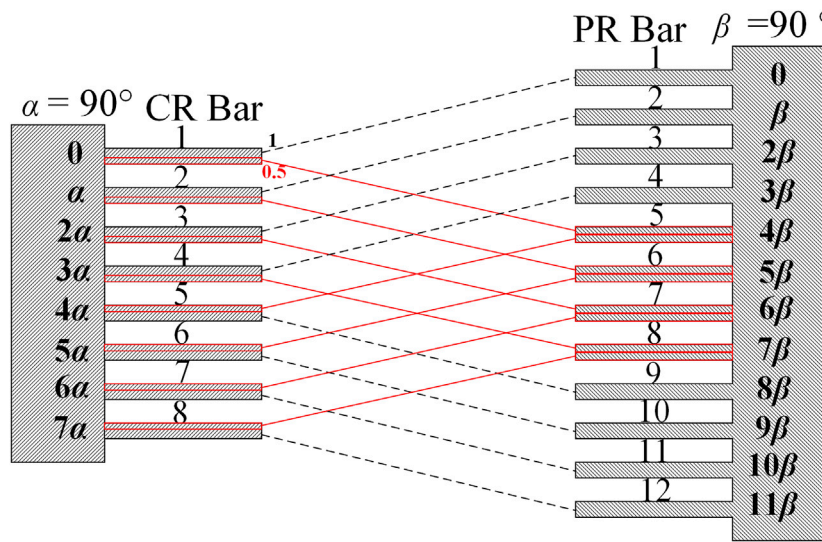


FIGURE 4 | Interconnection between PR bars (3 pole pairs and 12 slots) and CR bars (2 pole pairs and 8 slots).

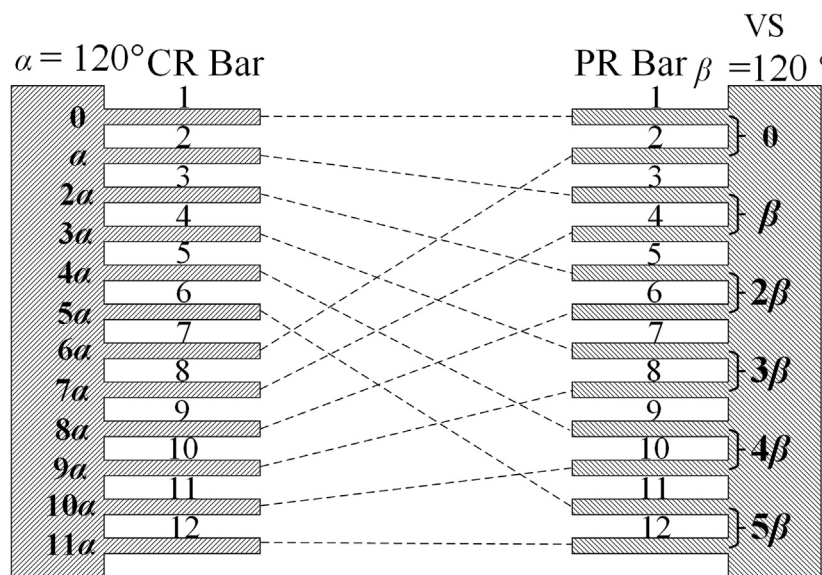


FIGURE 5 | Interconnection between PR bars (2 pole pairs, 12 slots and 6 VSs) and CR bars (4 pole pairs and 12 slots).

0.5, and they are marked by the dashed and solid wires, respectively. Every slot of the PR is arranged one conductor bar with 1 per unit area except the slots of No. 5 to No. 8. The slots of No. 5 to No. 8 all place two 0.5 per-unit-area conductor bars in parallel so that they are equivalent to the 1 per-unit-area in each slot, balancing with the other slots of the PR.

$$p_p = kp_c \text{ and } Z_p = Z_c$$

If the pole pairs of the PR are k multiples of the CR and their rotor slots are identical, the calculated values of α and β are unequal. The conductor bars of the PR and CR

cannot interconnect each other because of their different electrical phase angles of the slots. A method of the virtual slot (VS) is proposed to solve this problem, which enables the PR and CR to obtain the same electrical phase angle. The proposed method is illustrated as follows: k number of slots for the PR merge into one VS which occupies an electrical phase angle so that the number of VSs for the PR is k multiples of the number of real slots of the CR, while the pole pairs of the PR and CR are invariant. In this way, the electrical angles for the real slots of the CR and the VSs of the PR are identical.

TABLE 3 | Interconnection between PR and CR bars under PW with 2 pole pairs, CW with 1 pole pairs and rotor slots of 40.

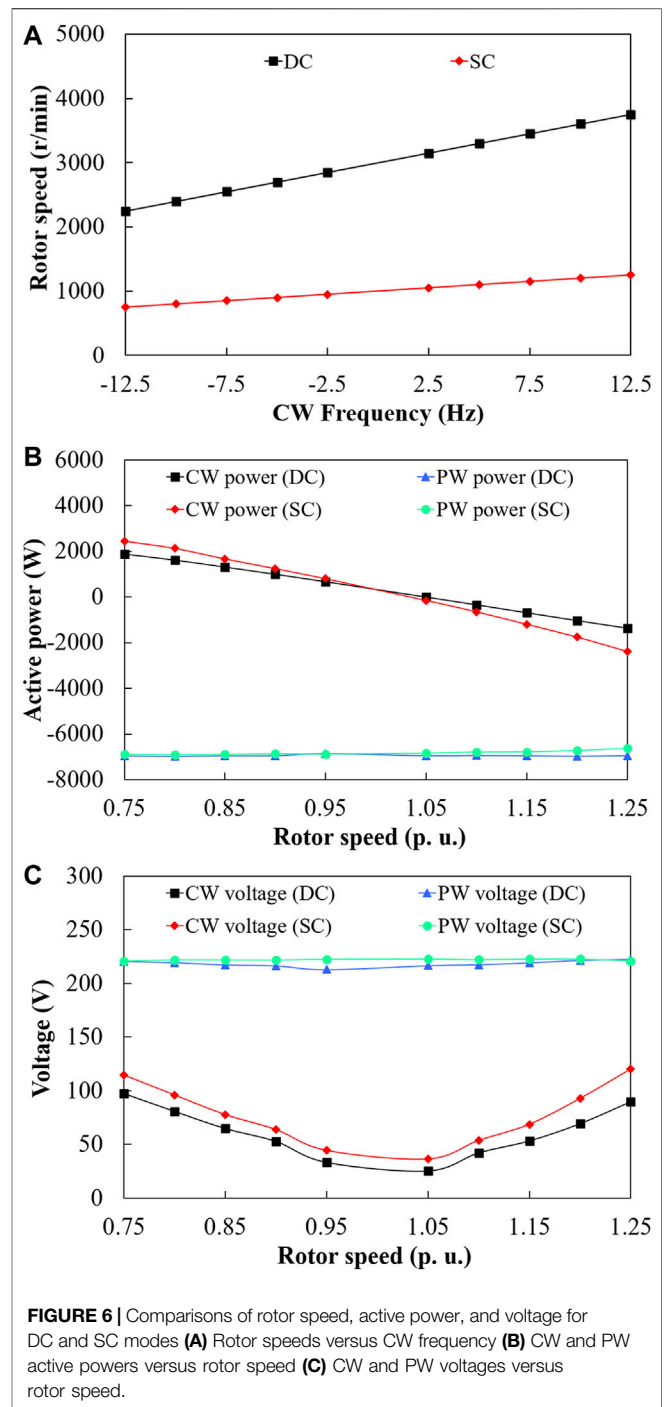
	CR		PR	
Pole pair	1		2	
Slot	40 (20 VSs)		40	
Electric phase angle	18°(VSs)		18°	
Group I	Bar No	α	Bar No	β
	1	0	1	0
	3	18	2	18
	5	36	3	36
	7	54	4	54
	9	72	5	72
	⋮	⋮	⋮	⋮
	33	288	17	288
	35	306	18	306
	37	324	19	324
	39	342	20	342
Group II	2	0	21	360
	4	18	22	378
	6	36	23	396
	8	54	24	414
	10	72	25	432
	⋮	⋮	⋮	⋮
	34	288	37	648
	36	306	38	666
	38	324	39	684
	40	342	40	702

Figure 5 shows the interconnection between the PR (2 pole pairs and 12 slots) and the CR (4 pole pairs and 12 slots) bars. Two real slots ($k = 1/2$) are merged into one VS of the PR, taking up the same electrical phase angle, and thus, connecting to two conductor bars of the CR. The conductor bars are supposed to be divided into four groups ($p_c = 4$) including group I (CR No. 1, 2, 3; PR No. 1, 3, 5), group II (CR No. 4, 5, 6; PR No. 7, 9, 11), group III (CR No. 7, 8, 9; PR No. 2, 4, 6), and group IV (CR No. 10, 11, 12; PR No. 8, 10, 12), and hence, avoiding plenty of interconnections of meaningless.

COMPARISON OF DS-BDFIM-SDCR WITH DC AND SC

Interconnection of DS-BDFIM-SDCR With DC

A DS-BDFIM-SDCR with the PW of 2 pole pairs and the CW of 1 pole pair based on the DC is modeled to validate the effectiveness of doubly-fed operation and predict the electromagnetic performance. The specification of the proposed machine is tabulated in Table 1 where shows the numbers of slots for the inner and outer rotors both of 40, conforming to the slot/pole combination of $p_p = kp_c$ and $Zp = Zc$. Since the electrical angles of the inner and outer rotors are not unequal, the VSM is utilized to solve the problem of interconnection. Two rotor slots of the inner rotor are regarded as one VS so that two conductor bars of the CR occupy the same electrical angle, connecting to the two slots of the outer rotor. The interconnection way of the PR and the CR is given in Table 3. Both electrical phase angles of the PR and the



CR are calculated to be 18° in terms of the PR with 2 pole pairs and 40 real slots and the CR with 1 pole pair and 20 VSs. Two groups should be divided ($k = 2$) and meaningless connections of different groups are forbidden. The odd and even NO. of CR bars are named by Groups I and II, respectively, and they both occupy a 2π period. According to the interconnection rule of Eq. 12, the PR bars are arranged in sequence to connect the same electrical phase angle of the CR bars.

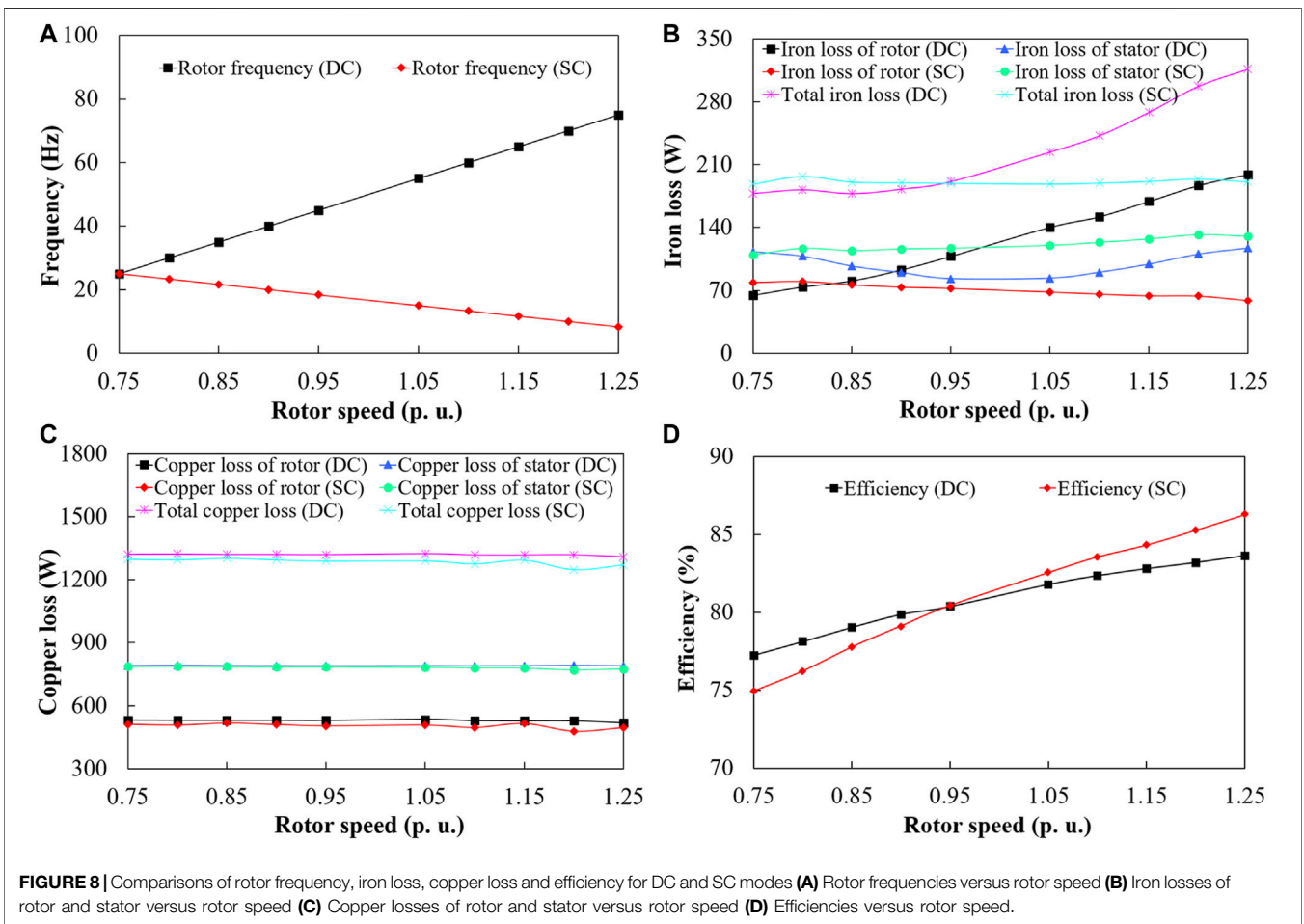
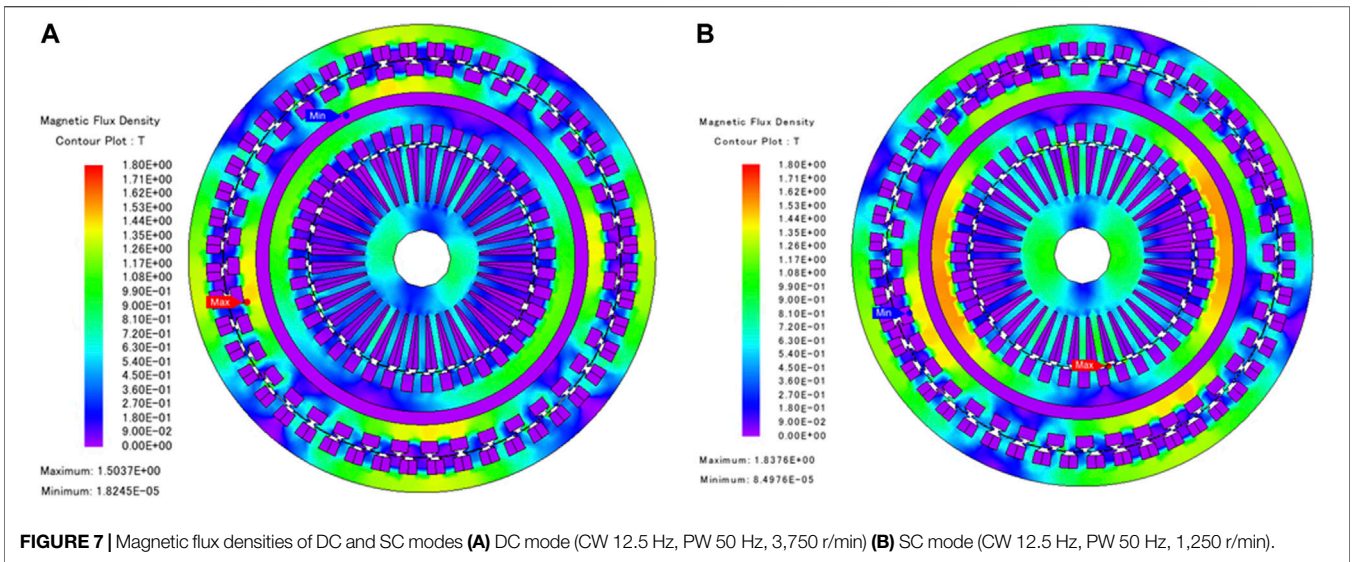


TABLE 4 | Performance comparison between DC and SC modes under rated sub-natural and super-natural synchronous speeds.

Mode	Sub-natural synchronous speed		Super-natural synchronous speed	
	DC	SC	DC	SC
Speed (r/min)	2,250	750	3,750	1,250
Load (Ω)	20	20	20	20
PW voltage (V)	220.4	220.6	222	220.85
PW current (A)	10.8	10.74	10.78	10.53
CW voltage (V)	99.2	114.8	90.4	120.3
CW current (A)	9.19	9.19	9.19	9.19
PW frequency (Hz)	50	50	50	50
CW frequency (Hz)	-12.5	-12.5	12.5	12.5
Rotor frequency (Hz)	25	25	75	8.33
Active power of PW (W)	-6,963	-6,894	-6,933	-6,633
Reactive power of PW (Var)	0	0	0	0
Power factor of PW	1	1	1	1
Active power of CW (W)	1867.5	2,449.5	-1,365	-2,390.1
Apparent power of CW (W)	2,734.9	3,165	-2,492.3	-3,316.67
Power factor of CW	0.68	0.75	0.548	0.72
Flux linkage of PW (Wb)	0.746	0.74	0.746	0.729
Flux linkage of CW (Wb)	0.91	1.16	0.997	1.47
Current of conductor bar (A)	232.6	225.7	230	219
Current of outer and inner end rings (A)	723/1,443	735/1,438	721/1,442	720/1,426
Resistance of PW (Ω)	1.32	1.32	1.32	1.32
Resistance of CW (Ω)	1.3	1.3	1.3	1.3
Resistance of rotor bar (Ω)	1.678e-4	1.678e-4	1.678e-4	1.678e-4
Resistance of inner end ring (Ω)	1.467e-6	1.467e-6	1.467e-6	1.467e-6
Resistance of outer end ring (Ω)	2.227e-6	2.227e-6	2.227e-6	2.227e-6
Copper loss of PW (W)	461.1	457.2	460.5	439.5
Copper loss of CW (W)	329.5	329.2	330.3	329.4
Copper loss of rotor (W)	558.2	510.8	518.7	478.4
Total copper loss (W)	1,348.8	1,297.4	1,309.5	1,247.3
Iron loss of inner stator (W)	10.2	11.6	12	17.1
Iron loss of outer stator (W)	25.3	26.5	72.7	24.9
Iron loss of inner rotor (W)	39.4	40.8	126.4	33.8
Iron loss of outer rotor (W)	103	97.9	105.3	113.1
Total iron loss (W)	177.9	176.8	316.4	188.9
Efficiency (%)	76.9	75.1	83.6	86.3

Performance Comparisons of DS-BDFIM-SDCR With DC and SC

The merits of the DS-BDFIM-SDCR based on the DC are the wide speed range and the high natural synchronous speed to obtain the comparable power density comparing to the SC mode, while the drawback of the DC mode is the increment of the loss, decreasing the efficiency of the machine. The performance comparisons of the DC and the SC for the DS-BDFIM-SDCR are discussed in this part to illustrate their characteristics. A DS-BDFIM-SDCR model with the PW of 2 pole pairs and the CW of 1 pole pair is adopted to predict the performance. The equivalent synchronous pole pairs based on the DC mode is 1 and those of the SC mode is 3. The rated CW frequency is selected to be ± 12.5 Hz so that the corresponding sub-natural synchronous and super-natural synchronous speeds of the DC mode are 2,250 and 3,750 r/min, while those of the SC mode are given by 750 and 1,250 r/min, respectively. The PW of the DS-BDFIM-SDCR, whose rated phase voltage is 220 V, connects a load of 20 Ω , outputting the rated electrical power of 7260 W. The CW is excited by the current source with the peak value of 13 A which keeps constant when the rotor speed changes. Besides, the numbers of slots for the inner stator, the outer stator and the

rotor are 48, 36, and 40, respectively, and more information is listed in **Table 1**.

Speed Range, Voltage and Power

The speed ranges of the DC and SC modes are determined by the equivalent synchronous pole pairs. The variable speed range of the DC mode is much higher than that of the SC mode as shown in **Figure 6A**, displaying that the speed range of the DC mode starts from 2,250 to 3,750 r/min, whereas that of the SC mode works the doubly-fed operation from 750 to 1,250 r/min during the variation of the CW frequency from -12.5 to 12.5 Hz. Actually, the DS-BDFIM-SDCR with DC is a high-speed-low-torque machine and the SC mode appears the characteristic of low-speed-high-torque.

Benefiting from the high operating speeds, the DC mode acquires the electrical power comparable to the SC mode and this is validated by **Figure 6B** which presents the absorbed or the output power of the PW and the CW. It is noted that the absorbed power of the winding is indicated by the positive value, while the minus values stand for the output power, and furthermore, the per-unit speed of the rotor is employed for graphing (3,000 r/min of the DC mode and 1,000 r/min of the SC mode both expressed by 1 p. u.). The CW absorbs the active power from the grid under the sub-natural synchronous speed and outputs the active power when the per-unit speed of the rotor is larger

TABLE 5 | Performance comparison between DS-BDFIM-SDCR and DS-BDFIM with wound rotor.

Mode	DS-BDFIM	DS-BDFIM-SDCR
	with wound rotor	
Mode	Differential mode	Differential mode
Speed (r/min)	3,750	3,750
Load (Ω)	20	20
PW voltage (V)	220.5	222
PW current (A)	10.85	10.78
PW frequency (Hz)	50	50
CW frequency (Hz)	12.5	12.5
Rotor frequency (Hz)	75	75
Active power of PW (W)	-7,068	-6,933
Reactive power of PW (Var)	0	0
Power factor of PW	1	1
Active power of CW (W)	-1,245	-1,365
Resistance of PW (Ω)	1.3	1.32
Resistance of CW (Ω)	1.51	1.3
Copper loss of PW (W)	459	460.5
Copper loss of CW (W)	342.6	330.3
Copper loss of rotor (W)	1,036.5	518.7
Total copper loss (W)	1838.1	1,309.5
Iron loss of inner stator (W)	29.2	12
Iron loss of outer stator (W)	112.8	72.7
Iron loss of inner rotor (W)	112	126.4
Iron loss of outer rotor (W)	172.9	105.3
Total iron loss (W)	426.9	316.4
Efficiency (%)	78.6	83.6

than 1, namely, the super-natural synchronous speed, both for the DC and the SC modes. As the rotor speed increases, the absolute CW power initially reduces and then rises because the CW frequency declines and then grows up, and simultaneously, the PW features the constant active power outputs. The absolute CW power of the DC is always lower than that of the SC in a variety of speeds, implying that the total active power outputs of the DC at sub-natural synchronous speeds are higher than that of the SC, while they are evidently low under super-natural synchronous speeds comparing to the SC mode.

Figure 6C reveals the variation of the CW and PW voltages at various rotor speeds for the DC and SC modes. The phase voltages of the PW stay 220 V both for the DC and SC though there is a little fluctuation for the DC mode. The CW voltages of the DC and the SC gradually decrease and then increase, along with the increment of the rotor speed. The nearer to the natural-synchronous speed, the lower CW voltage needs and the lower CW power factor appears. The CW voltage of the SC is higher than the DC one at the full speed range owing to the fact that the absolute power of the CW for the SC mode is higher than that of the DC mode as shown in **Figure 6B**. Also, the magnetic flux density of **Figure 7** shows that the inner stator and rotor of the SC mode have a higher value than those of the DC mode, and thus, more CW voltages for excitation.

Rotor Frequency, Iron Loss, Copper Loss and Efficiency

The other aspect that should be discussed between the DC and SC modes is their difference in the rotor frequency and what consequences it causes.

Figure 8A shows the rotor frequencies of the DC and SC modes vary with the rotor speeds. As the rotor speed increases, the rotor frequency of the DC mode grows up, while that of the SC mode declines. Evidently, at the super-natural synchronous speed, the rotor frequency of the DC mode is much larger than the SC one, especially for the rated rotor speed of 1.25 p. u. The expressions of the rotor frequency based on the DC mode at the sub-natural and super-natural synchronous speeds are respectively given by

$$f_r = \begin{cases} \frac{f_p + f_c}{|p_p - p_c|} p_p - f_p & n > 1 \text{ p.u.} \\ \frac{f_p - f_c}{|p_p - p_c|} p_p - f_p & n < 1 \text{ p.u.} \end{cases} \quad (18)$$

The rotor frequency of the SC modes can be deduced by

$$f_r = \begin{cases} f_p - \frac{f_p + f_c}{p_p + p_c} p_p & n > 1 \text{ p.u.} \\ f_p - \frac{f_p - f_c}{p_p + p_c} p_p & n < 1 \text{ p.u.} \end{cases} \quad (19)$$

Figure 8B compares the iron losses of the rotor and the stator as well as the total losses for the DC and SC modes. The rotor iron losses of the DC are much higher than those of the SC at different speeds because the DC mode suffers from the high rotor frequency except the low speed of 0.75 p. u. where the rotor frequencies of the DC and SC modes are the same. The iron loss is not only determined by the rotor frequency but also the magnetic flux density so that the iron losses of the SC stator are higher than those of the DC stator at full range speeds due to the higher magnetic flux density of the SC stator as shown in **Figure 7**. As a result of a mix of the rotor frequency and the magnetic flux density, the total losses of the DC mode are greatly higher than the SC one at the super-natural synchronous speeds, while they are below the SC mode at the sub-natural synchronous speeds.

The copper losses of the rotor and stator versus the rotor speed for the DC and SC modes are compared in **Figure 8C**, showing that the copper losses of the DC and SC stators are almost the same, whereas those of the SC rotor are lower than the those of the DC rotor due to the higher rotor frequency for the DC. However, their difference seems to be small because the maximum rotor frequency of the DC mode is only 75 Hz which lays a small impact on the copper loss. Therefore, the total copper loss of the DC shows a little bit bigger than that of the SC.

Figure 8D exhibits the efficiencies at various rotor speeds under the DC and SC modes. The efficiencies of the DC mode are superior to those of the SC mode at the sub-natural synchronous speeds, while at the super-natural synchronous speeds they are worse. The significant reason for the DC mode with higher efficiency at the sub-natural synchronous speeds comparing to the SC mode is that the DC mode offers lower CW voltage, thus reducing the absorbed power and increasing the total power outputs. At the super-natural synchronous speeds, the DC mode

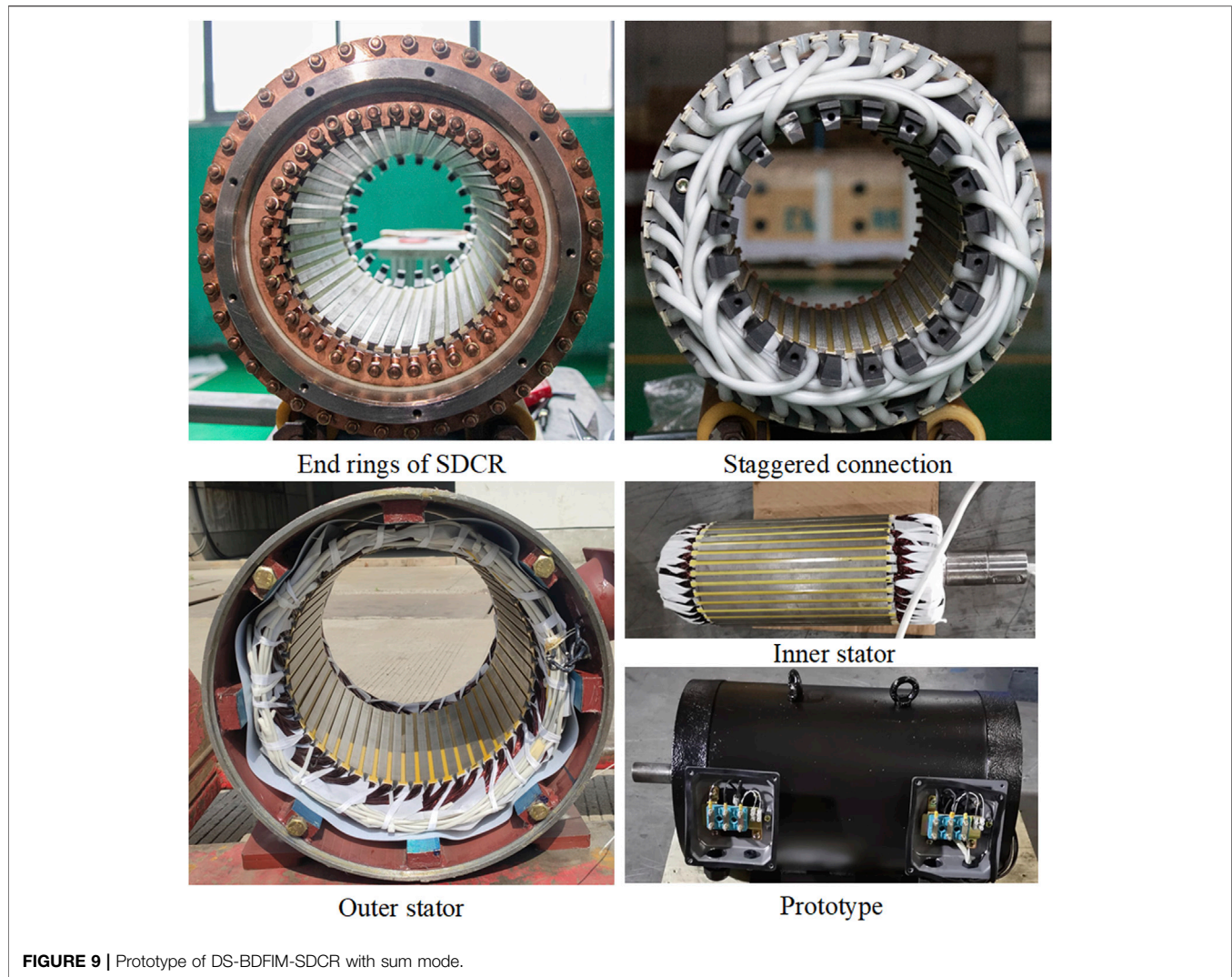


FIGURE 9 | Prototype of DS-BDFIM-SDCR with sum mode.

has higher rotor frequencies than the SC mode, and thus higher rotor iron losses, higher copper losses as well as lower efficiencies.

Table 4 tabulates the detailed performance comparison between the DC and SC modes under rated sub-natural and super-natural synchronous speeds. The efficiency calculation of the DS-BDFIM-SDCR is given by

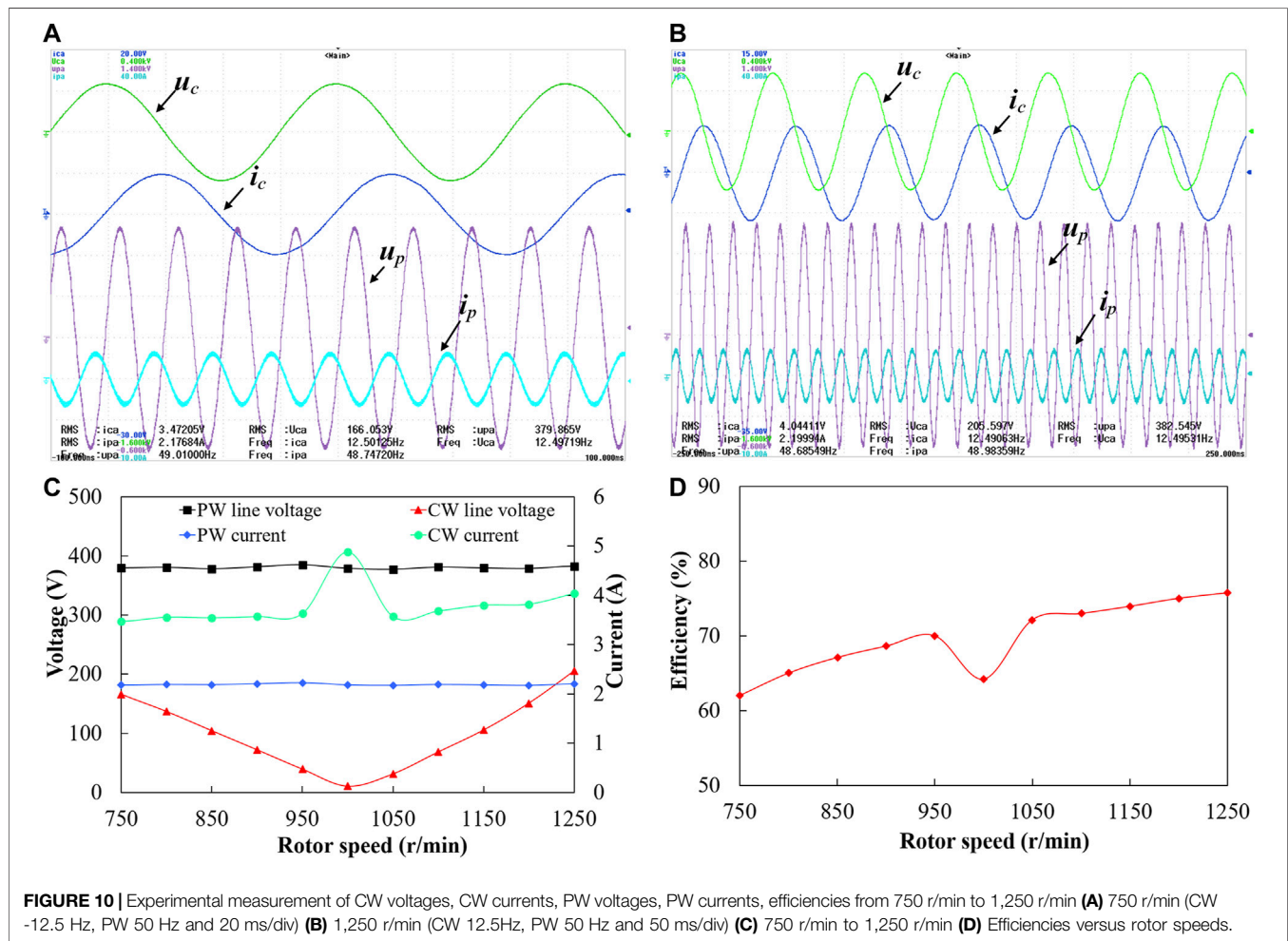
$$\eta = \frac{P_p + P_c}{P_p + P_c + P_{iron} + P_{copper}} \quad (20)$$

where P_p and P_c are the outputted or absorbed powers, while P_{iron} and P_{copper} are the total copper loss and total iron loss of the machine, respectively.

When the DC mode with 2,250 r/min and the SC mode with 750 r/min, their rotor frequencies are the same, resulting in the same total iron losses (177.9 and 176.8 W, respectively) approximately. Since the absorbed active power of the CW based on the DC mode (1867.5 W) is significantly lower than that of the SC one (2,449.5 W), the DC mode (76.9%) performs more efficiently comparing to the SC mode (75.1%). The DC

mode with the rotor frequency of 75 Hz (at 3,750 r/min) brings about the iron loss of 316.4 W, while the SC mode with the rotor frequency of 8.33 Hz (at 1,250 r/min) leads to the iron loss of 188.9 W, contributing the higher efficiency of the SC mode (86.3%) than the DC mode (83.6%). To sum up, it can be concluded that the DC mode behaves better than the SC mode at sub-natural synchronous speed, but its iron and copper losses at super-natural synchronous speed are supposed to be further optimized.

To validate the superiority of the DS-BDFIM-SDCR with the differential mode, the performance comparison between the DS-BDFIM-SDCR and the DS-BDFIM with wound rotor in (Han et al., 2017) is shown in **Table 5**. The copper loss of the PW and CW between the two machines are similar, however, the copper loss of the rotor for the DS-BDFIM with wound rotor is almost twice of the DS-BDFIM-SDCR ones, verifying the advantages of the low resistance of squirrel cage rotor comparing to the wound rotor. Furthermore, the total iron loss of the DS-BDFIM with wound rotor is also higher than that of the DS-BDFIM-SDCR.



Therefore, the DS-BDFIM-SDCR based on the differential modes with the efficiency of 83.6% is obviously higher than the efficiency of 78.6% for the DS-BDFIM with wound rotor.

EXPERIMENT

The DS-BDFIM-SDCR with sum mode is prototyped as shown in Figure 9. The core component of the prototype is the SDCR, one end of which is short-circuited by two copper rings, while the other end is formed by the staggered connection. Since the copper bars are hard to achieve the staggered interconnection in the end when the prototype is manufacturing, they are replaced by soft parallel enameled wires so as to facilitate implementation.

The CW with the excitation of the voltage source and the PW with a load of $100\ \Omega$ to enable the prototype of the doubly-fed operation. Figures 10A,B shows the measured PW voltages (50 Hz), CW voltages (± 12.5 Hz), PW currents and CW currents at 750 and 1,250 r/min. To obtain the rated PW line voltage of 380 V, the CW is excited with the root mean square (RMS) line voltages of 166 V at 750 r/min, and 205.6 V at 1,250 r/

min, respectively. The waveforms of the PW voltages and currents exhibit sinusoidal distributions, verifying the low harmonics of the DS-BDFIM-SDCR.

The voltages and currents of both PW and CW versus the rotor speeds from 750 to 1,250 r/min are measured in Figure 10C. The PW line voltages at different speeds stay the same of 380 V. The CW voltage declines initially and then grows up. As the speed increases, the CW current exhibits a small change except for the natural-synchronous speed of 1,000 r/min where the direct source is excited, while the PW current maintains the same due to the constant resistance load. The experimental measurement of efficiency versus rotor speeds from 750 to 1,250 r/min is given in Figure 10D, showing the efficiencies increases along with the rotor speeds except for the natural speed of 1,000 r/min.

CONCLUSION

In this article, the design method of the DC for the DS-BDFIM-SDCR is proposed to solve the issues of high rotor leakage and

low capacity of magnetic field conversion of the conventional differential-mode-based BDFM. The proposed method enables the high number of conductor bars for the cage rotor even with the low synchronous pole pairs of $[p_1-p_2]$, achieving reduced rotor flux leakage. The rotating MMF theory is utilized to deduce the conditions that should be satisfied for the SDCR. Based on the result of derivation, two situations of pole/slot combinations are taken into account and examples are illustrated to introduce the details of interconnection of the SDCR. The FE models of the DS-BDFIM-SDCR with DC and SC are built to compare their electromagnetic performance. The results show that the DC mode of the DS-BDFIM-SDCR exhibits better performance than the SC one at the sub-synchronous-speed region such as lower CW excitation, lower iron loss and higher efficiency, while at the super synchronous-speed region, the DC mode suffers from higher copper loss and iron loss due to the increased rotor frequency comparing to the SC mode, and hence, lower efficiency. Therefore, the iron and copper losses are ought to be further optimized.

REFERENCES

- Cheng, M., and Zhu, Y. (2014). The State of the Art of Wind Energy Conversion Systems and Technologies: a Review. *Eng. Convers. Manag.* 88, 332–347. doi:10.1016/j.enconman.2014.08.037
- Cheng, Y., Yu, B., Kan, C., and Wang, X. (2020). Design and Performance Study of a Brushless Doubly Fed Generator Based on Differential Modulation. *IEEE Trans. Ind. Electron.* 67, 10024–10034. doi:10.1109/TIE.2019.2962430
- Han, P., Cheng, M., Ademi, S., and Jovanovic, M. G. (2018). Brushless Doubly-Fed Machines: Opportunities and Challenges. *Chin. J. Electr. Eng.* 4, 1–17. doi:10.23919/cjee.2018.8409345
- Han, P., Cheng, M., Jiang, Y., and Chen, Z. (2017). Torque/power Density Optimization of a Dual-Stator Brushless Doubly-Fed Induction Generator for Wind Power Application. *IEEE Trans. Ind. Electron.* 64, 9864–9875. doi:10.1109/TIE.2017.2726964
- Li, H., Liu, H., and Xu, B. (2019). “A New Experimental Method of Brushless Doubly-Fed Machine Based on Differential Mode,” in 2019 IEEE 8th Joint International Information Technology and Artificial Intelligence Conference (ITAIC) (IEEE), 1159–1163. doi:10.1109/itaic.2019.8785732
- Okedu, K. E., Ai Tobi, M., and Ai Araithi, S. (2021). Comparative Study of the Effects of Machine Parameters on DFIG and PMSG Variable Speed Wind Turbines during Grid Fault. *Front. Energ. Res.* 9, 1–13. doi:10.3389/fenrg.2021.655051
- Pan, W., Chen, X., and Wang, X. (2021). Generalized Design Method of the Three-phase Y-Connected Wound Rotor for Both Additive Modulation and Differential Modulation Brushless Doubly Fed Machines. *IEEE Trans. Energ. Convers.* 36, 1940–1952. doi:10.1109/TEC.2020.3045061
- Roberts, P. C. (2004). *A Study of Brushless Doubly-Fed (Induction) Machines*. Cambridge: University of Cambridge.
- Ruviaró, M., Runcos, F., Sadowski, N., and Borges, I. M. (2012). Analysis and Test Results of a Brushless Doubly Fed Induction Machine with Rotary Transformer. *IEEE Trans. Ind. Electron.* 59, 2670–2677. doi:10.1109/TIE.2011.2165457
- Shiyi Shao, S., Abdi, E., and McMahan, R. (2012). Low-cost Variable Speed Drive Based on a Brushless Doubly-Fed Motor and a Fractional Unidirectional Converter. *IEEE Trans. Ind. Electron.* 59, 317–325. doi:10.1109/TIE.2011.2138672
- Williamson, S., Ferreira, A. C., and Wallace, A. K. (1997). Generalised Theory of the Brushless Doubly-Fed Machine. Part 1: Analysis. *IEE Proc. Electr. Power Appl.* 144, 111–122. doi:10.1049/ip-epa:19971051
- Xiong, L., Liu, X., Liu, Y., and Zhuo, F. (2020). “Modeling and Stability Issues of Voltage-Source Converter Dominated Power Systems: a Review,” in *CSEE*

DATA AVAILABILITY STATEMENT

The original contributions presented in the study are included in the article/supplementary material, further inquiries can be directed to the corresponding author.

AUTHOR CONTRIBUTIONS

YZ did the conceptual design, simulation analysis and writing of the paper. MC revised and improved the article. XY and CZ organized case studies.

FUNDING

This work was supported in part by the National Natural Science Foundation of China (NSFC) under Grant 61973073 and the Scientific Research Foundation of Graduate School of Southeast University under Project YBPY 1878.

Journal of Power and Energy Systems (IEEE), 1–18. doi:10.17775/CSEEJPES.2020.03590

- Yin, J. (2021). Research on Short-Circuit Current Calculation Method of Doubly-Fed Wind Turbines Considering Rotor Dynamic Process. *Front. Energ. Res.* 9, 1–7. doi:10.3389/fenrg.2021.686146
- Zeng, Y., Cheng, M., Wei, X., and Xu, L. (2020). Dynamic Modeling and Performance Analysis with Iron Saturation for Dual-Stator Brushless Doubly Fed Induction Generator. *IEEE Trans. Energ. Convers.* 35, 260–270. doi:10.1109/TEC.2019.2942379
- Zeng, Y., Cheng, M., Wei, X., and Zhang, G. (2021). Grid-connected and Standalone Control for Dual-Stator Brushless Doubly Fed Induction Generator. *IEEE Trans. Ind. Electron.* 68, 9196–9206. doi:10.1109/TIE.2020.3028824
- Zhang, F., Yu, S., Wang, Y., Jin, S., and Jovanovic, M. G. (2019). Design and Performance Comparisons of Brushless Doubly Fed Generators with Different Rotor Structures. *IEEE Trans. Ind. Electron.* 66, 631–640. doi:10.1109/TIE.2018.2811379
- Zhang, K., Zhou, B., Or, S. W., Li, C., Chung, C. Y., and Voropai, N. I. (2021). “Optimal Coordinated Control of Multi-Renewable-To-Hydrogen Production System for Hydrogen Fueling Stations,” in *IEEE Transactions on Industry Applications (Early Access)* (IEEE), 1. doi:10.1109/TIA.2021.3093841

Conflict of Interest: The authors declare that the research was conducted in the absence of any commercial or financial relationships that could be construed as a potential conflict of interest.

The reviewer QW declared a shared affiliation with the authors YZ, MC, XY, CZ to the handling editor at the time of the review.

Publisher’s Note: All claims expressed in this article are solely those of the authors and do not necessarily represent those of their affiliated organizations, or those of the publisher, the editors and the reviewers. Any product that may be evaluated in this article, or claim that may be made by its manufacturer, is not guaranteed or endorsed by the publisher.

Copyright © 2021 Zeng, Cheng, Yan and Zhang. This is an open-access article distributed under the terms of the Creative Commons Attribution License (CC BY). The use, distribution or reproduction in other forums is permitted, provided the original author(s) and the copyright owner(s) are credited and that the original publication in this journal is cited, in accordance with accepted academic practice. No use, distribution or reproduction is permitted which does not comply with these terms.